

Manifestation of quantum chaos on ordered structures by scattering techniques: application to Low-Energy Electron Diffraction

P. L. de Andres and J. A. Vergés

Instituto de Ciencia de Materiales de Madrid, Consejo Superior de Investigaciones Científicas, Cantoblanco, E-28049 Madrid, Spain

(November 17, 2017)

We analyze statistical probability distributions of intensities collected by diffraction techniques like Low-Energy Electron Diffraction. A simple theoretical model based in hard-sphere potentials and LEED formalism is investigated for different values of relevant parameters: energy, angle of incidence, muffin-tin potential radius, maximum spherical component l_{max} , number of stacked layers, and full multiple-scattering or kinematic model. Given a complex enough system (e.g., including multiple scattering by at least two Bravais lattices), the computed probability distributions agree rather well with a χ_2^2 one, characteristic of the Gaussian Unitary Ensemble universality class associated to quantum chaos. A hypothesis on the possible impact of the chaoticity of wavefunctions on correlation factors is tested against the behaviour of the Pendry R-factor and the Root Mean Squared Deviation factor.

61.14.-x, 05.45.+b, 61.14.Hg

I. INTRODUCTION

There is much interest to understand the role of chaos on quantum systems. The important consequences of chaos on classical systems yield a clear motivation to extend the study of chaos to the quantum physics world. It is difficult, however, to explore quantum chaos by connecting the quantum and classical formulation through some special limits¹. Therefore, a group of pioneering investigators adopted long time ago a point of view well independent of any classical or semiclassical approach to chaos². In this approach, the object of interest is a Hamiltonian composed of random numbers (RMT)^{3,4}, conjectured by Wigner, Dyson and others to be a relevant prototype for quantum chaotic behaviour. A further conjecture by Porter and Thomas⁵ established the probability distribution to be expected for intensities related to a typical chaotic wavefunction: χ_ν^2 . This is a function that gives the probability distribution of intensities $I / \langle I \rangle$, over the spatial support of the wavefunction at a given energy ($\langle I \rangle$ is the corresponding mean value). Later on, Dyson demonstrated that the parameter ν can only take three different values (i.e., 1, 2, and 4, depending on the Hamiltonian to be constructed with real, complex or quaternions numbers). On the other hand, starting from a semiclassical analysis, Berry suggested that a typical wavefunction for a chaotic system could be formed by an infinite superposition of plane waves travelling in random directions and with random phases⁶. Working with

this important conjecture, Berry was able to show that the probability distribution for those wave functions is $P(I / \langle I \rangle) = e^{-I / \langle I \rangle}$, with $I = \psi\psi^*$, and that the space-averaged spatial correlation of the wavefunction (at a fixed energy) is proportional to the zeroth order integer Bessel function. Finally, the application of a supersymmetry formalism has produced a rigorous deduction of the probability distributions associated to a non-linear supermatrix sigma-model⁷, that under certain assumptions can be shown to be equivalent to RMT and results in the Porter-Thomas distribution⁸.

It is clear that RMT bears some limitations, specially derived from its statistical nature. However, it has the advantage of providing a clear object to be studied and a corresponding well defined methodology. In this paper, we adopt this statistical approach, and having in mind the results from RMT we study the probability distributions associated to wave functions relevant for popular surface structure techniques, like Low-Energy Electron Diffraction (LEED) or X-ray Photo-Electron Diffraction (PED). Wavefunctions have a potentially higher information content than the mere inspection of levels, and they are also the natural objects to be studied in these techniques. We find that the computed probability distributions match closely the statistics of the eigenfunctions of a Hamiltonian belonging to the Gaussian Unitary Ensemble (GUE). This is the universality class relevant to a scattering experiment, i.e., to an open geometry, where the energy takes values in the continuum (good quantum numbers characterizing the wavefunction are the energy and k_{\parallel} to the surface). Therefore, we take a fresh look to the physical system and advance the hypothesis that the good structural sensitivity of these techniques can be understood as a manifestation of quantum chaos on the wavefunctions. This conjecture is tested for two standard correlation factors widely used to measure the *distance* between a reference structure (usually the experimental one) and a trial one calculated theoretically. The results point in the same direction as the statistical analysis of wavefunctions since we find that there is a region where the correlation factor grows at an exponential rate.

Even if our analysis is not directly linked to any classical analysis, it is worth mentioning that, the classical analogue of every quantum system we have considered behaves chaotically due to the intrinsic complexity of the many-scatterer problem^{6,9}. Furthermore, it is interesting to notice that the classical problem might behave chaotically even if the scatterers are regularly distributed.

Therefore, it is surprising to find such a vast literature on quantum chaos related to some kind of disorder, but such a little consideration of ordered systems, because using the classical analogue to guide intuition, it is not clear why quantum chaos should not to be found in perfectly ordered systems. Recently, Mucciolo et al.¹⁰ have shown that the high energy region of the calculated band structure of crystalline Si is complex enough to follow the statistical distribution of levels expected for the Gaussian Orthogonal Ensemble (GOE) universality class. Inspired by these ideas, we have also presented a preliminary work studying the statistical properties of LEED states¹¹ on ordered materials. Of course, the LEED problem is quite related to the band structure analysis, its main advantage being merely practical because of the ready availability of experimental data to test new theoretical findings.

Berry has studied the Sinai's billiard by mapping the problem to a periodic array of hard-circles on a plane¹². This problem can be solved efficiently applying a Korringa-Kohn-Rostoker formalism. His method not only has a number of computational advantages, but also allows a detailed analysis for the different role played by nonisolated and isolated orbits contributing to the wavefunctions. It is interesting to notice that the nonisolated orbits add to the complexity of the system through the boundaries defining the billiard only. Therefore, although their role is non-negligible to determine the chaoticity of the levels in the closed system, they do not contribute to the open problem of scattering. In other words, paths that never strike a disk do not contribute to the reflectivity of a surface (like in LEED) or they are deliberately removed from the analysis (like in PED or DLEED) due to their lack of useful structural information. In scattering experiments, these paths would be characterized by a probability distribution given by χ_∞^2 (a Dirac's delta function). Therefore, the study of an open system allows quite naturally to separate the influence of nonisolated and isolated orbits, because the nonisolated ones yield only a trivial contribution, in contradistinction with the essential entanglement between both types in the bound problem.

The organization of this paper is as follows: the scattering of a plane wave by an ordered array of hard-sphere potentials is analyzed in section II in detail applying a LEED formalism. This is a good analogue to Berry's work on Sinai's billiard from a scattering point of view, although some important differences remain (e.g., it is a genuine three-dimensional system). The hard-sphere model is interesting from a theoretical point of view because of the strong similarity with the billiard problem, and also because its analysis uses the same basic tools employed in the solution of the diffraction by a surface. Certainly, the usual approach to the LEED problem¹³ starts computing the diffraction matrices for a single layer, and then it proceeds stacking layers by different methods. In practice, that means solving first the multiple scattering problem *inside* a layer, to solve later on the multiple scattering problem *between* layers through a

stacking process that finally recreates the material bulk, or at least a thick enough slab. The use of hard-sphere potentials simplifies the computational problem allowing the identification of the key physical elements responsible for the appearance of the Porter-Thomas probability distribution. Following the strategy of introducing complexity step by step, we start computing the reflection and transmission matrices for one layer of hard-sphere potentials. Those layers are afterwards stacked to form an fcc crystal with an arbitrary lattice parameter borrowed from copper. Section III gives a similar analysis for a LEED problem trying to represent realistically a few selected materials. Results corresponding to both Diffuse LEED (DLEED) and conventional I(E) analysis are discussed in this part. Finally, we consider in section IV the impact of our previous findings on the statistical correlation factors (R-factors) widely used in LEED or PED to assess the confidence on a structure predicted by theory. This is usually done by a trial and error fit, comparing theoretically calculated diffracted intensities with the experiment. The usual rules are as simple as: (i) the lower the R-factor the better, and (ii) it should represent a (hopefully global) minimum. In practice, because there is no way to secure a real global minimum in a multi-dimensional parameter space, the recipe of getting a low-enough value becomes the only guide to trust or not a given structure. We shall see how a new criterion adding to the others can be obtained by identifying the existence of a region where the R-factor changes quickly (exponentially) from values typically obtained from the application of perturbation theory ($R \approx 0$) to values representative for uncorrelated intensities ($R \approx 1$). We argue that this exponential dependence is a consequence of the chaotic nature of wave functions obtained in a complicated multiple-scattering scenario.

II. SIMPLIFIED MODEL OF ELECTRON MULTIPLE SCATTERING BY N-SCATTERER: HARD-SPHERE POTENTIALS

A. Scattering by an isolated potential

We analyze first the simplest case related to our problem: the scattering of a plane wave, e^{ikz} , by a single atomic potential modelled by a hard-sphere of radius R ¹⁴. The scattered wave is given asymptotically by:

$$e^{ikz} + f_k(\theta) \frac{e^{ikr}}{r} \quad (1)$$

with

$$f_k(\theta) = \frac{1}{k} \sum_{l=0, \infty} \sqrt{4\pi(2l+1)} t_l(k) Y_{l0}(\theta) \quad (2)$$

where,

$$t_l(k) = e^{i\delta_l} \sin(\delta_l) ,$$

and¹⁵

$$\delta_l(k) = \arctan[(-1)^{l-1} \frac{J_{l+\frac{1}{2}}(kR)}{J_{-l-\frac{1}{2}}(kR)}].$$

Fig. 1 displays the probability distribution function for intensities scattered by this model at constant energy when the angle θ is varied. This is compared with the Porter-Thomas law characteristic of a chaotic system to stress the different statistical behaviour. Only two parameters are relevant to this experiment: the length scale ($R = 2$ a.u.), and the energy scale. The approximate semiclassical rule $kR \approx l_{max}$ gives us some rough value for the maximum component in the spherical wave expansion, and twice that value is used in all our calculations ($l_{max} = 20$). Because the phase-shifts bring some non-trivial dependence on kR through the spherical Bessel functions, results for three different energy values spanning the range of interest are given to illustrate this dependence. Basically, the same statistical pattern is found, reflecting the smooth variation of the scattering factor (moduled by the forward peak). This probability distribution is remarkably similar to the one found for the typical wave function of a chaotic system when too few random components are used¹¹.

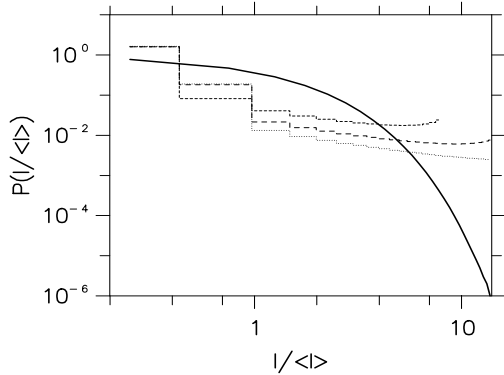


FIG. 1. Probability distribution for the scattering of a plane wave by a single hard-sphere potential ($R=2$ a.u.). Three energies (in a.u.) are shown: $E = 2$ (short dashed), $E = 5$ (long dashed), and $E = 10$ (dotted). The thick solid line is the χ_2^2 function corresponding to the GUE wavefunctions statistics.

B. Electron diffraction by a plane of scatterers

The same statistical probability distribution is expected for the diffraction of a single Bravais lattice in the kinematical approximation at normal incidence, where all the atoms scatter the plane-wave at the same time and are equivalent because of the Bravais-like symmetry. In this approximation, the lattice is merely contributing a structure factor composed of delta functions centered around Bragg conditions¹⁶. However, by taking an appropriate limit on the full dynamical result, we shall see that this is not the case when the angle of incidence is

varied (cf. Figure 4), because of the $n \times \sin(\theta)$ extra path added to each scatterer in the plane ($n = 0, \infty$).

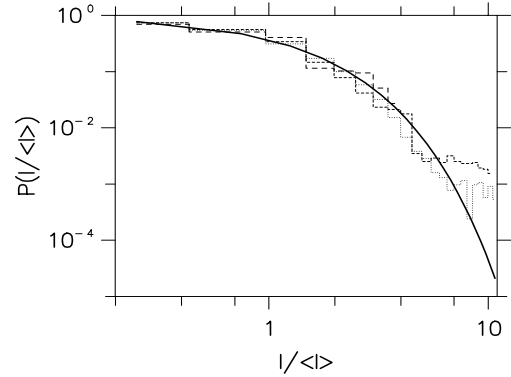


FIG. 2. Probability distribution of wavefunctions reflected by one layer of hard-spheres potentials. Results for $R = 2$ a.u. and three different energies are shown: $E = 2$ a.u. (long dashed), 5 a.u. (short dashed), and 10 a.u. (dotted).

To proceed gradually from simple to more complicated systems, we now analyze the diffraction matrix of a single two-dimensional Bravais lattice^{13,16,17}:

$$M_{\vec{K}_{g'}^{\pm}, \vec{K}_g^{\pm}} = \frac{8\pi^2 i}{|\vec{K}_g^{\pm}| |\vec{K}_{g'}^{\pm}|} \sum_{lm, l'm'} e^{i\delta_{l'}} \sin(\delta_{l'}) \times \{i^{l'} (-1)^m Y_{l-m}(\vec{K}_g^{\pm})\} \frac{1}{(1-X)_{lm, l'm'}} \{i^{-l'} Y_{l'm'}(\vec{K}_{g'}^{\pm})\} \quad (3)$$

This expression gives the complex amplitude diffracted from an ingoing beam, \vec{K}_g^{\pm} , into an outgoing one, $\vec{K}_{g'}^{\pm}$. Therefore, it is the basic quantity needed to compute the reflection, $R = M^{+, -}$ and transmission, $T = I + M^{+, +}$, of just one layer (where $-$ denotes propagation towards the vacuum where the original wave was originated, and $+$ in the opposite direction).

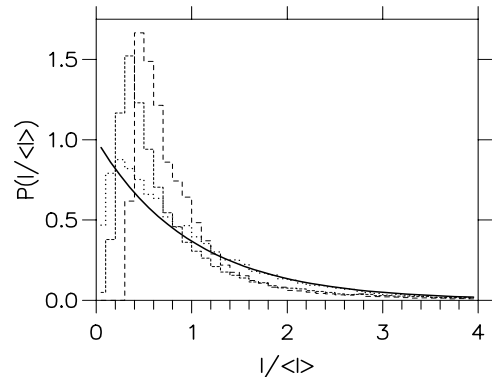


FIG. 3. Dependence of the wavefunction probability distribution on the hard-sphere radius. Results for $E = 10$ a.u. and $R = 2.0$ a.u. (dotted), 0.2 a.u. (dashed) and, 0.02 a.u. (long-dashed) are shown.

Fig. 2 shows the wavefunction statistical distributions obtained for a two-dimensional square lattice of hard-

sphere potentials at nearest-neighbours distances taken from a Cu(100) surface (4.82 a.u.). Internal parameters relevant for the calculation are kept to the same values as the preceding case ($R = 2$ a.u., and $l_{max} = 20$). An arbitrarily small positive imaginary part V_{oi} is added to the energy to give the Green's functions the required analytical behaviour. The physical effect of such a mathematical trick is to ensure the proper decay of waves at infinity. The actual value used in our calculations is $V_{oi} = 0.001$ a.u., small enough compared with all relevant energies as not to have any noticeable effect (Kambe's method¹⁸ is used to compute the lattice summation and about 2300 lattice points are included). Given these values for the internal parameters of the model, intensities still depend on external parameters that typically will be explored in real experiments: the energy, and the incident and collection angles. In our previous work¹¹ we have studied the statistical probability distribution in scattering intensities varying the collection angle (Diffuse LEED) and the energy (standard I(E) LEED analysis), but at a fixed incident angle defined by θ and ϕ . In this paper, we increase the database size by considering different initial incident directions on a solid angle centered around $\theta = 0^\circ$ and $30^\circ - 40^\circ$ degrees wide. As the energy is the main external parameter controlling the experiment in any case, results for three different energies spanning the range of interest ($E = 2, 5$ and 10 a.u.) are systematically shown for comparison. We remark that the trivial limit χ_∞^2 , is recovered at fixed energy from Equation (3) for $l_{max} = 0$, or alternatively when $R \rightarrow 0$, that eventually would make only one spherical component necessary, killing all the dependence on the angles θ or ϕ . None of the parameters used in our model correspond to unrealistic values regarding real LEED experiments, except for the very small imaginary part for the optical potential. In a typical LEED experiment the inelastic interaction is strong, concentrating the diffraction process to the vicinity of the surface (which explains the sensitivity of the experiment to small atomic displacements in the few last layers). This can be taken into account effectively including a large optical potential ($\approx 0.1 - 0.2$ a.u.) in the energy. However, it is important to realize that the experiment is conceived as purely elastic, and electrons having lost some energy do not contribute to the detected intensity. Realistic values have been previously used to make contact with experiments¹¹, and now we choose to work in the limit $V_{oi} \rightarrow 0$ to show that this value is not controlling the resulting probability distributions in any way. The actual computer code used is a modern version of routines given by Pendry¹³. Figure 2 clearly shows how the single Bravais layer gives diffracted intensities that already have statistical distributions close to the ideal Porter-Thomas law, irrespectively of the energy.

Next, the energy is fixed at some arbitrary representative value ($E = 10$ a.u.), and the dependence of the statistical probability distribution of a two-dimensional Bravais lattice on the size of the hard-sphere potential is studied. Fig. 3 gives the statistics for three different

sizes of the hard-sphere radius. As $R \rightarrow 0$, the reflected intensities also become negligible. From a computational point of view, we do not expect this limit to be strictly accessible for a numerical experiment, because the computer zero, determined by a numerical underflow, might be contaminated by round-off errors with a statistical distribution not known *a priori*. Average values for the intensities at $E = 10$ a.u. are 1.6×10^{-2} , 2.5×10^{-4} , and 4.1×10^{-6} , respectively for $R = 2, 0.2$, and 0.02 (a.u.). Figure 3 shows the tendency of the probability distribution towards χ_∞^2 , associated with the constant value corresponding to very small radius value. As the main interest in this case is to show the behaviour near the origin, we have skipped the usual log-log plot, well suited to manifest the fast exponential decay, but not so useful to stress the behaviour near the origin.

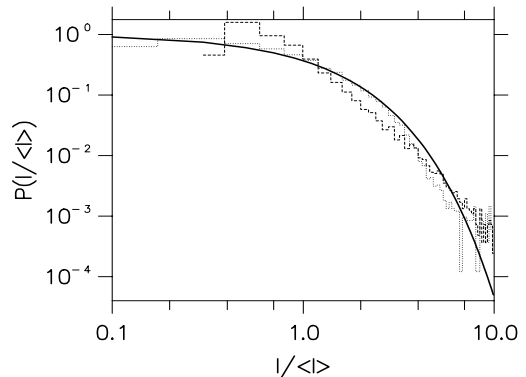


FIG. 4. Full dynamical model for a single Bravais lattice (dotted) compared to a kinematic one (dashed). Parameters for the calculation are: $E = 10$ a.u., $R = 2$ a.u., and $l_{max} = 20$.

To understand the role of the complexity created by the intralayer multiple-scattering versus the geometrical factor of different incident angles, we have artificially made the intralayer scattering matrix equal to zero: $X = 0$. The result is shown in Fig. 4 for fixed values of E , R , and l_{max} . It is observed that the kinematic N-scatterer problem analyzed for different incident angles, already approximates the Porter-Thomas distribution, although the inclusion of intralayer multiple scattering gives a distribution closer to the ideal one.

C. Electron diffraction by a stacking of planes of hard-spheres scatterers

We use the *layer doubling* scheme¹³ to stack layers of hard-sphere potentials. Layers are stacked to form an fcc lattice, borrowing the intralayer distances from copper, as before. Taking into account the small imaginary part used in our calculations, we should at least double the width of the slab up to distances of about $l_c \approx \frac{\sqrt{2E}}{V_{oi}}$, approximately including 1000 layers. This is not practical, nor necessary, and we only slowly double the slab

size to investigate the influence of the layer width on the statistical distribution.

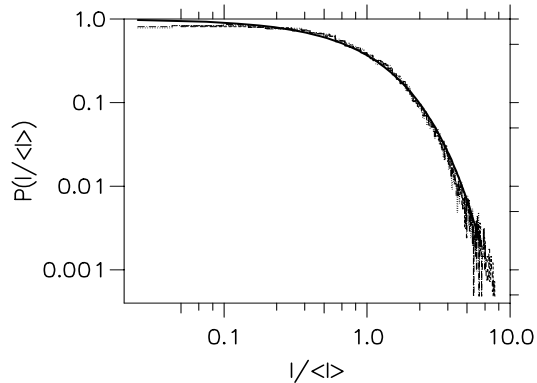


FIG. 5. Reflected intensities statistics of a full dynamical calculation of a slab of increasing width: The number of stacked layers is 2 (dotted), 4 (dashed), 8 (long-dashed) and, 16 (double-dashed double-dotted). Other computational parameters are given in the previous figure caption.

This is illustrated in Fig. 5 for four different widths: 2, 4, 8 and 16 layers (for comparison, the result for 1 layer can be found in Fig. 4). Other parameters are fixed to the same values previously used to isolate features only associated to the slab width. It is easily appreciated how the statistical distribution tends more to behave like the ideal Porter-Thomas one as the width is increased. It is difficult to mathematically quantify this tendency, but an approximate way would be to make a least-squares fit of the data to χ^2_ν functions, and give the ν with the best agreement. This results in $\nu = 2.7, 2.3, 2.2, 2.2$, and 2.2 for 1, 2, 4, 8 and 16 layers respectively. The mean values of the intensity reflected are for each case: 1.58×10^{-2} , 2.42×10^{-2} , 2.55×10^{-2} , 2.58×10^{-2} , and 2.58×10^{-2} . A penetration depth of sixteen layers is to be thought as a practical upper limit for most experimental systems. From these numbers, it must be concluded that, at least under the particular conditions we have chosen, *intralayer* scattering among the first two layers help the distribution most to compare well with the Porter-Thomas law, while further stacking of layers mainly contributes to improve the finer details. Therefore, a moderate amount of multiple scattering should be generically held responsible for the statistical behaviour of wave functions, characteristic of quantum chaos.

III. APPLICATION TO DIFFUSE AND CONVENTIONAL I(E) LEED ANALYSIS

All these ideas can be used to analyze LEED experiments conducted in standard surface structural analysis. Those experiments are performed by measuring as a function of the energy, the available exiting beams (I(E) standard LEED) or by analyzing many different exiting beams at a few fixed energies (DLEED). The former tech-

nique is usually applied to ordered surfaces, while the latter is more appropriated to surfaces with disorder. As the relevant physical principles behind both techniques are the same, and are well described by a multiple scattering formalism, it is not surprising to find that both intensities, the ones simulated theoretically for realistic systems, and the corresponding to experimental measured values, fit rather well to the Porter-Thomas distribution. Indeed, the main differences with our previous model are the atomic potentials and the important electron-electron inelastic interaction that attenuates the wave within a few layers of the surface. While our results are not very sensitive to a particular set of phase-shifts, as become obvious from our results for different materials simulated with realistic potentials, the influence of a large optical potential is balanced by our finding that scattering by one, or two layers at most, is enough to reproduce the characteristic GUE probability distribution.

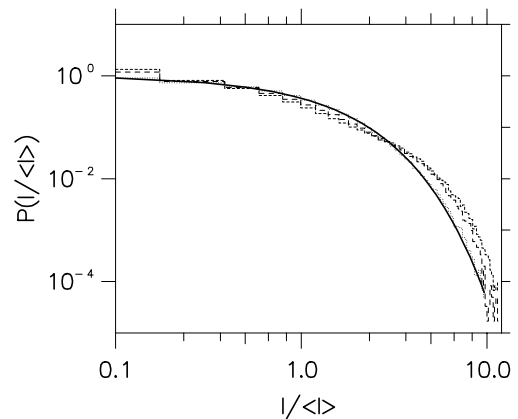


FIG. 6. Probability distribution for DLEED intensities of O/Ni(100). $E = 12$ a.u. (dotted), 14 a.u. (short dashed), and 16 a.u. (long dashed).

This is demonstrated in Figures We first explore the statistical behaviour of DLEED. A representative system many times considered in the literature both from the experimental and the theoretical point of view is the lattice gas disordered adsorption of oxygen on Ni(100)¹⁹. Nickel is obviously a strong scatterer and multiple-scattering plays an important role. This is relevant because the adsorbate is both illuminated directly by the wave coming from the electron gun and by the reflected wave coming from the surface, that depends on energy and angle in a complicated manner dictated by the multiple scattering inside the substrate. Geometrical parameters are taken from a detailed structural search, fixing the adsorption position at about 1.5 a.u. on the four-fold symmetry position in the square surface lattice (less symmetric adsorption sites would only make more complex the system and therefore more likely to recover the Porter-Thomas law). Three different energies are computed theoretically using a dynamical approach at $T = 0$ K, as described by Saldin and Pendry²⁰. To improve the statistics, differ-

ent incident angles θ and ϕ are computed and used as explained above. The agreement with Porter-Thomas is quite good (e.g., $E = 12$ a.u. gives a least-squares fit ν value of 2.0), reflecting that although the diffuse background is generated by scattering with only one atom responsible for breaking the otherwise perfect symmetry that would result in Bragg conditions, the wave reflected by the substrate and illuminating the atom is very complicated. Obviously that what matters most here is that the forward scattering of that wave by the adsorbate is stronger or comparable to the backscattering of the simple plane wave by the same potential.

Our previous findings can also be corroborated analyzing experimental DLEED intensities measured for the same system by the Erlangen group²¹. Figure 7 shows such an analysis for five different energies going from $E = 3.7$ a.u. to $E = 11.1$ a.u. in approximate steps of 1.8 a.u. The database was measured in a sample cooled down to liquid Nitrogen temperature (≈ 90 K), at normal incidence, and for an approximate coverage of 0.25 (1 representing one full monolayer adsorbed). Less than one thirtieth of the amount of data used in the theoretical analysis is available, making a poorer statistics, but the expected tendency is followed well, although fluctuations are clearly observed.

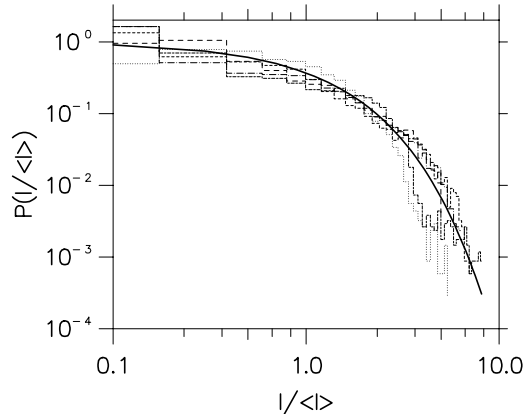


FIG. 7. Probability distribution for experimental DLEED intensities of O/Ni(100). $E = 3.7$ a.u. (dotted), 5.6 a.u. (short dashed), 7.5 a.u. (long dashed), 9.4 a.u. (long dashed-dotted), and 11.1 a.u. (long dashed-short dashed).

We have also analyzed the experimental data measured by the Erlangen group on the system: K/Ni(100) -disordered-. Normal incidence and liquid Nitrogen cooling ($T = 90$ K) are used again. Potassium coverage is kept at a lower value of 0.05. This system, however, shows an important difference with the last one: Potassium is adsorbed at the hollow site, but at a much higher position, ≈ 5.1 a.u. It is clear that the source of complexity is the substrate, and if the atom would be isolated, or too far away from the surface, the DLEED intensities would simply correspond to the ones due to a single atomic potential. From our previous estimate for

the typical decaying length, we find that $l_c \approx 15 - 20$ a.u. for the energies involved in the experimental data. Therefore, it is not unexpected that the probability distribution for K/Ni(100) bear some similarity to the one obtained for an isolated atom, as can be seen in Figure 8.

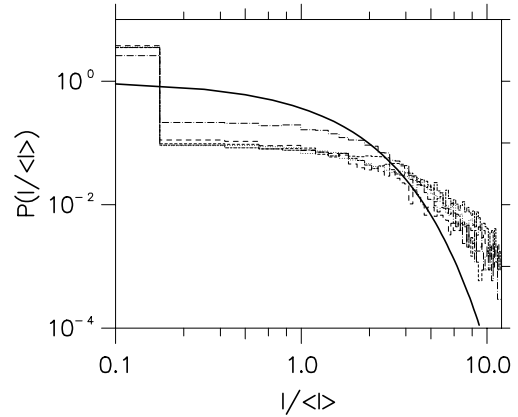


FIG. 8. Probability distribution for experimental DLEED intensities of K/Ni(100). $E = 3.7$ a.u. (dotted), 5.6 a.u. (short dashed), 7.5 a.u. (long dashed), 9.4 a.u. (long dashed-dotted), and 11.1 a.u. (long dashed-short dashed).

By reference to the RMT, or to Berry's hypothesis about the structure of the typical wavefunction on a chaotic system, it is clear that the same Porter-Thomas law should manifest if intensities are analyzed as a function of energy at a fixed arbitrary position, \vec{r} . We have analyzed this behaviour for scattering wavefunctions by calculating LEED I(E) curves for three materials not bearing a structural, nor an electronic relationship: Cu(100), W(100) and Si(111), and by analyzing a real LEED experiment. Figure 9 shows the probability distributions computed for Cu(100), and Figure 10 gives the same result for W(100), Si(111) and experimental data for $c(8 \times 2)$ GaAs(100). The Van Hove-Tong LEED package is used to compute intensities within the Renormalized Forward Scattering (RFS) approximation to describe multiple scattering between layers, and realistic phase-shifts representing the atomic potentials are considered²². To improve the statistical confidence of the results, we chose an arbitrary azimuthal angle (not related to any symmetry direction) of $\phi = 30^\circ$, and we explore a range of polar angles from $\theta = 5^\circ$ to $\theta = 40^\circ$, in steps of $\theta = 5^\circ$. The first 9 emergent beams over an energy range from $E = 2$ to 20 a.u. are considered and other parameters relevant for the calculation are: $l_{max} = 7$, $V_{oi} = .15$ a.u., $T = 0$ K, and up to a maximum of 101 beams included. For copper, we consider two different distances between the first and the second surface layers, $d_{12} = 3.4$ a.u. and 3.02, corresponding respectively to the perfect unrelaxed surface and to the experimental relaxation found on clean Cu(100) crystals. Both cases are seen (cf. Figure 9) to be well represented

by the χ_2^2 probability distribution. An average of intensities for different samples with d_{12} values going from 3.02 to 3.74 in steps of 0.08 a.u. is also considered with a similar result. In addition, we compute for an hypothetical relaxation of $d_{12} = 2.0$ a.u., where the RFS technique is used outside its validity region and it results in unphysical divergences. The statistical distribution associated with this absurd case is seen to be very different from the previous ones, signaling clearly that something went wrong in the calculation. This is an extreme situation, but the same we have been able to detect a theoretical problem with a simple statistical analysis, the Porter-Thomas distribution may help to identify cases where gross experimental systematic errors, like an improper subtraction of the background, saturation of some bright beams, etc, occur. We have repeated a similar theoretical analysis for W(100) and Si(111) surfaces in Figure 10. While similar conditions are used for W(100), owing to experimental practical difficulties to measure the high energy end in semiconductors, we use a smaller energy range for Si(111) (from 1. to 11 a.u.), but the first 13 emerging beams are considered to have a database with a similar size to the one considered for the metals.

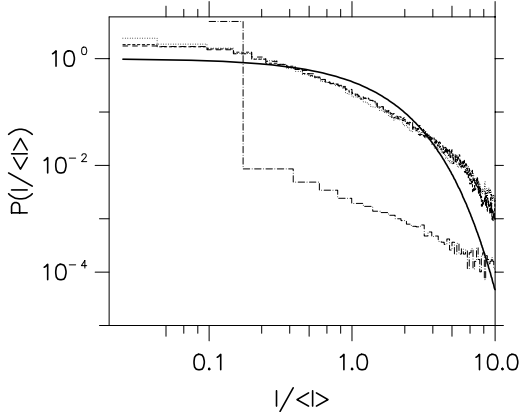


FIG. 9. Probability distribution corresponding to the LEED I(E) curves for Cu(100). considering different surface relaxations, $d_{12} = 3.40$ a.u. (dotted), $d_{12} = 3.02$ a.u. (short dashed), an equally weighted average from 3.02 to 3.74 (long dashed), and $d_{12} = 2.00$ a.u. (dotted-dashed).

Although agreement between the multiple-scattering calculations and experimental data is very good for geometries representing well a given surface (e.g., Pendry R-factor for the structural analysis of Cu(100) is already below 0.1, and experimental and theoretical I(E) curves are hardly distinguishable by simple ocular inspection), we also take into account experimental intensities from the $c(8 \times 2)$ -GaAs(100) reconstruction²³. Nineteen independent beams measured at normal incidence, and giving an approximated energy range of 86 a.u. are considered. Intensities have been digitalized from the published results, and interpolated with splines in such a way that the interpolated curves cannot be distinguished by eye from

the measured data. Again, a fair agreement between the obtained probability distributions and the ideal Porter-Thomas law is obtained, although we observe that the agreement is achieved over a limited range due to the smaller amount of available data.

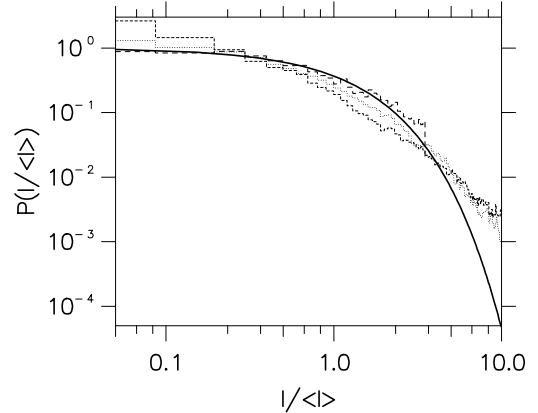


FIG. 10. Probability distribution corresponding to the LEED I(E) curves for W(100) (dotted), Si(111) (dashed) and $c(8 \times 2)$ -GaAs(100) (long dashed).

IV. R-FACTORS DEPENDENCE ON GEOMETRICAL STRUCTURAL PARAMETERS

An interesting question derived from the chaotic nature of the wave function is how quickly two given structures differing in a given structural parameter, p , become unrelated from the point of view of diffracted intensities. This process happens, although the two structures are always related through some underlying geometrical relationship, via the complexity introduced by multiple scattering. To demonstrate this point, we first analyze theoretically computed diffracted intensities where only one relevant parameter is varied. Afterwards, we apply the same ideas to a recent structural search on an experimental system performed by other people²⁴. The theoretical experiment is performed using the same DLEED program mentioned before²⁰. This allows us to simulate the adsorption of an oxygen atom on the hollow site of a perfect (unrelaxed) Ni(100) surface. The reference height is fixed again at 1.5 a.u. from the layer defined by the nickel cores, which is very similar to the experimental value. Changing the oxygen adsorption height we study the corresponding changes in the DLEED intensities. We notice that the same code has been previously used for a real structural search on this system, proving its capability to give a realistic description of the physical system¹⁹.

To measure the changes in the LEED diffracted intensities we adopt two common but otherwise unrelated correlation factors: (i) the Root Mean Squared Deviation R_{RMSD} ¹⁶, and (ii) the Pendry R-factor, R_P ²⁵. The former is the simplest choice at hand, and we apply it to the DLEED theoretical experiment:

$$R_{RMSD} = \sqrt{\frac{1}{N} \sum_{k=1, N} (I_k^{ref} - I_k)^2} \quad (4)$$

where k labels the different $\vec{k}_{\parallel, out}$. This R-factor is conveniently normalized to $\frac{1}{\sqrt{N}}$, the value expected for two random sets of intensities with the same average value (intensities are normalized to their average value). On the other hand, the Pendry R-factor is a very common choice in standard structural analysis of I(E) LEED curves, and because it was used by Polop et al.²⁴ in their study of the $c(2 \times 2)$ -Si/Cu(110), we simply analyze the behaviour of their published values. The fact that we find the same type of behaviour with two so different R-factors supports our hypothesis that the effects discussed in this section are quite general.

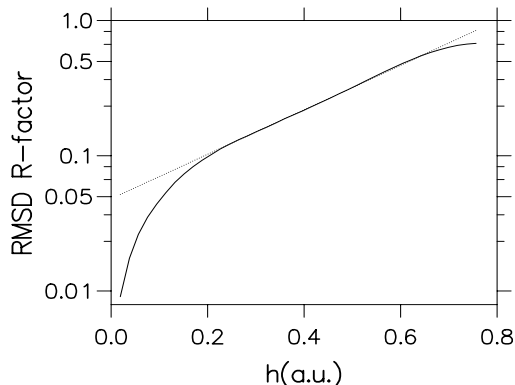


FIG. 11. Root mean square deviation (R_2) measuring the correlation between a reference structure, $S(0)$, and a family of structures labelled by the adsorption height of an atom, $S(h)$. Region II (see text) is shown as the linear region (in logarithmic scale) between the minimum (region I) and the saturation region (region III). Energy is fixed to 2.0 a.u.

In a previous publication¹¹, we have distinguished the existence of three different regions in parameter space, P : (I) a perturbative region, characterized by a polynomial dependence, $R(p) \propto p^n$; (II) an exponential region, $R(p) \propto e^p$, where small changes in a given structural parameter result in rapidly increasing R-values; and (III) a fully chaotic region where the R-factor saturates approximately to the values expected for the comparison between two randomly generated structures (by definition ≈ 1 in both R-factors used here). Beyond these regions, the existence of multiple coincidence minima recreates again similar, although more imperfect conditions²⁶. Existence of region I is justified by the applicability of perturbative techniques like Tensor LEED. The range of validity of the simplest version of perturbation theory (e.g., Tensor LEED in its first form, where the perturbing potential upon displacement of one atom is simply proportional to that displacement) is known by common experience on different systems to be ≈ 0.2 a.u.²⁷. It is interesting to notice that more sophisticated versions of TLEED could extend their range of validity to $\approx 0.4 - 0.6$ a.u., being practically impossible to extend the use of pertur-

bation theory beyond 0.8 a.u. We remark that those displacements correspond typically to R-factors between the reference structure (by definition $R = 0$) and the one to be computed perturbatively of about $R = 0.2 - 0.4$. In the examples presented below (figures 11 and 12), we observe that this normally corresponds to a region where the R-factor change exponentially with the structural parameter. Therefore, it is possible to understand why perturbation theory completely breaks within this region in spite of the considerable effort that has been made to apply it²⁸.

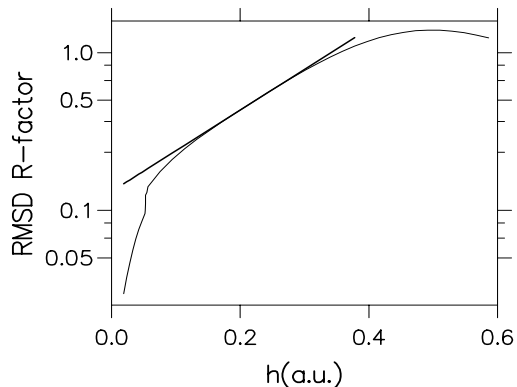


FIG. 12. Same results as presented in

The existence of region II is illustrated in figures 11, and 12 with theoretically simulated data, and in 13 with data produced by comparing with the experiments. Regarding the theoretical simulation, we have slowly increased the adsorption height of the oxygen atom to get a corresponding increasing in the R_2 . To show the functional dependence between R_2 and h , we take logarithms in the ordinate axis and we identify a region where the curve can be approximated very well by a straight line. This region should be considered the onset of quantum chaos, and therefore a region of dubious value for structural work.

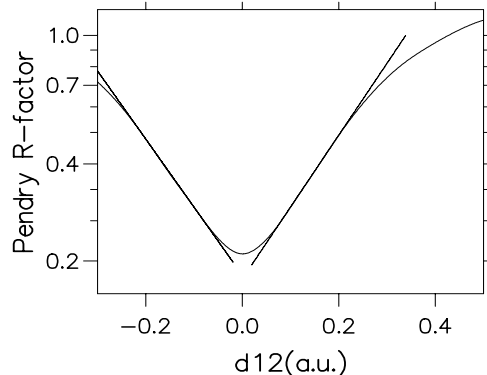


FIG. 13. The Pendry R-factor is analyzed in a similar way to R_{RMSD} in Figure 11. Data corresponding to an experimental structural analysis by I(E) LEED of $c(2 \times 2)$ Si/Cu(110) is considered.

To test whether this behaviour is particular to a given

definition of the R-factor or not, we perform the same analysis using the Pendry R-factor. This function is defined in very different terms to the simpler root mean squared R_2 considered above. However, Fig. 13 shows the same type of behaviour for R_P . This corresponds to R-factors comparing structural models to experimental data for a recent structural search performed on the system $c(2 \times 2)\text{Si}/\text{Cu}(110)$ using conventional $I(E)$ curves²⁴. R_P is studied as a function of the two outer inter-layer distance, d_{12} , where the best value provided by the structural work has been subtracted to put the origin at $d_{12} = 0$.

V. CONCLUSIONS

Scattering intensities have been analyzed from a statistical point of view. The computed probability distributions compare well with the Porter-Thomas law, typical of random wavefunctions. To understand the origin of such a similarity we have analyzed models with increasing scattering complexity, using a hard-sphere approximation for the interaction potentials. The simplest case found displaying a statistical distribution similar to the Porter-Thomas law is single scattering by a Bravais lattice of N-scatterers at an arbitrary angle of incidence. When more complexity is added to the system (e.g., considering intra-layer multiple scattering, or multiple scattering between a few layers through a *layer doubling* stacking strategy), the statistical distribution of such idealized systems shows better agreement with the ideal χ_2^2 function. The same behaviour is found if realistic potentials are considered to describe the atoms within the periodic lattice. The analysis of real experimental data is also consistent with the same ideas, as expected from the known reliability of those theoretical methods to give scattering intensities if the geometries are already known. Finally, we have found that standard R-factors behave exponentially in a transition region (II), before the intrinsic complexity of multiple scattering effectively decouples wavefunctions for different geometrical structures. The existence of this region allows us to use concepts borrowed from classical chaos, and to propose a new criterion for the reliability of a given minimum in the R-factor, depending on whether the structure lies in a perturbative region (I), or beyond the transition zone (III).

VI. ACKNOWLEDGMENTS

This work has been supported by the CICYT under contracts num. PB96-0085 and PB97-1224. We are grateful with Prof. K. Heinz for making available to us the experimental DLEED data.

- ¹ M.V. Berry, in *Chaos and Quantum Physics*, edited by M.J. Giannoni, A. Voros and J. Zinn-Justin (Elsevier, 1991), pag. 251.
- ² e.g. see *Statistical Theories of Spectra: Fluctuations*, Ed. by C.E. Porter, Academic Press (New York, 1965).
- ³ M.L. Mehta, *Random Matrices*, 2nd ed. (Academic Press, San Diego, CA, 1991).
- ⁴ T.A. Brody, J. Flores, J.B. French, P.A. Mello, A. Pandey, S.S.M. Wong, *Rev. of Mod. Phys.* **53**, 385 (1981).
- ⁵ C.E. Porter, R.G. Thomas, *Phys. Rev.* **104**, 483 (1956).
- ⁶ M. Berry, *Semiclassical Mechanics of Regular and Irregular Motion*, in *Chaotic Behaviour of Deterministic Systems*, 171. Les Houches Lectures XXXVI, eds. G. Iooss, R.H.G. Helleman, R. Stora (North-Holland, Amsterdam, 1983).
- ⁷ K.B. Efetov *Supersymmetry in Disorder and Chaos* Cambridge Univ. Press (Cambridge, 1997).
- ⁸ V. I. Fal'ko and K. B. Efetov, *Phys. Rev. B* **52**, 17413 (1995).
- ⁹ M.C. Gutzwiller, *Chaos in Classical and Quantum Mechanics*, Springer Verlag (New York, 1990).
- ¹⁰ E.R. Mucciolo, R.B. Capaz, B.L. Altshuler, J.D. Joannopoulos, *Phys. Rev. B* **50**, 8245 (1994).
- ¹¹ P.L. de Andres and J.A. Vergés, *Phys. Rev. Lett.* **80**, 980 (1998).
- ¹² M. Berry, *Ann. Phys.* **131**, 163 (1981).
- ¹³ J.B. Pendry, *Low Energy Electron Diffraction*, Academic Press (London, 1974).
- ¹⁴ $\hbar = m_e = e = 1$ is used throughout the paper (i.e., energy is expressed in Hartrees, 27.2 eV, and distances in Bohrs, 0.0529 nm).
- ¹⁵ N.F. Mott and H.S.W. Massey, *The Theory of Atomic Collisions*, Oxford University Press 1965.
- ¹⁶ M.A. Van Hove, W.H. Weinberg and C.M. Chan, *Low-Energy Electron Diffraction*, (Springer-Verlag, Berlin, 1986).
- ¹⁷ J.L. Beeby, *J. Phys. C* **1**, 82 (1968).
- ¹⁸ K. Kambe, *Z. Naturforsch.* **23a**, 1280 (1968).
- ¹⁹ U. Starke, P.L. de Andres, D.K. Saldin, K. Heinz and J.B. Pendry, *Phys. Rev. B*, **38**, 12277 (1988).
- ²⁰ J.B. Pendry and D.K. Saldin, *Surf. Sci.* **145**, 33 (1984); D.K. Saldin and J.B. Pendry, *Comput. Phys. Commun.* **42**, 399 (1986).
- ²¹ K. Heinz, private communication.
- ²² M.A. Van Hove and S.Y. Tong, *Surface Crystallography by LEED*, (Springer-Verlag, Berlin, 1979)
- ²³ F.J. Palomares, Ph.D. thesis, Chap. 3 (pg. 66), Universidad Autonoma de Madrid, Madrid (1993).
- ²⁴ C. Polop, C. Rojas, E. Roman, J.A. Martin-Gago, B. Brena, D. Cocco, G. Paolucci, *Surf Sci* (in press).
- ²⁵ J.B. Pendry, *J. Phys. C: Solid State Phys.* **13** (1980) 937.
- ²⁶ S. Andersson, J.B. Pendry, *Solid State Commun.* **16**, 563 (1975).
- ²⁷ P.J. Rous, J.B. Pendry, D.K. Saldin, K. Heinz, K. Müller, N. Bickel, *Phys. Rev. Lett.* **57** 2951 (1986); P.J. Rous, Ph.D. thesis, Chap. 6 (pg. 167), Imperial College of Science, Technology and Medicine, London (1986).
- ²⁸ W. Oed, P.J. Rous, J.B. Pendry, *Surf. Sci.* **273**, 261 (1992).